ELSEVIER

Physica E 11 (2001) 245–251

PHYSICA E

www.elsevier.com/locate/physe

Confinement effects in crystallization and Er doping of Si nanostructures

M. Zacharias[a,*], J. Heitmann[a], M. Schmidt[b], P. Streitenberger[b]

[a] *Max-Planck-Institut für Mikrostrukturphysik, Weinberg 2, 06120 Halle, Germany*
[b] *Institut für Experimentelle Physik, Otto-von-Guericke Universität, PF 4120, 39016 Magdeburg, Germany*

Abstract

This article presents our comprehensive investigation of the crystallization of amorphous silicon films with a layer thickness below 20 nm from an experimental as well as from a theoretical point of view. The exponential scaling of the crystallization temperature with layer thickness is derived by using solid state crystallization theory. The critical height of the nanocrystals embedded in such superlattice structures depends on the specific interface free energies of the respective phases (oxide, amorphous Si, and crystalline Si) and exponentially on the layer thickness. In addition, strong enhancement of room temperature luminescence from Er ions embedded in the vicinity of Si nanocrystals is shown. Spatially resolved photoluminescence investigations and Rutherford backscattering measurements for Si and Er distributions along the same line scan clearly manifest that inhomogeneities in implantation are not the cause of the correlated increase of Er and decrease of nc-Si luminescence. However, this effect can be understood as a coupling of radiative processes, which includes an energy transfer from Si nanocrystals to Er ions.

PACS: 61.72.V; 61.43; 78.66.H

Keywords: Silicon; Erbium; Nanocrystals; Crystallization; Luminescence

1. Introduction

Nanoscaled structures are playing a major role in optoelectronic and semiconductor research with many applications already in commercial state. However, scaling down in dimension may lead to tremendous changes of the physical properties of such structures. New research fields, such as electronic confinement in low dimensional structures or photon confinement in photonic crystals, may be developed with high impact in the semiconductor device industry. Ultra-large scale integration technology is applied today for both active and passive components. For device application precise engineering of nanocrystal size is essential. Very recently, even optical amplification in Si nanocrystals has been reported [1]. With regard to the visible

* Corresponding author. Tel.: +49-345-5582-729; fax: +49-391-5582-557.
E-mail address: zacharias@mpi-halle.de (M. Zacharias).

1386-9477/01/$ - see front matter
PII: S1386-9477(01)00212-0

luminescence of nanocrystalline Si (nc-Si) the control of size, passivation and arrangement of Si nanocrystals embedded in an oxide matrix is mandatory. The structural confinement of thin Si films in Si/SiO_2 superlattices (SL) represents a new way to control arrangement as well as size of the nanocrystals [2,3].

The kinetics of the amorphous to polycrystalline transition has to be reviewed in view of understanding of the crystallization process in the limit of very thin films. With only a few atomic Si layers structural confined between a thin oxide the existing models for kinetic mechanisms of crystal grain growth are not applicable anymore. In the presence of multiple stacks of Si/SiO_2 periods, the amorphous-to-crystalline phase transition occurs through random nucleation of crystalline clusters surrounded by amorphous material under the strain field of the superlattice structure and the oxide boundary. Compared to a solid bulk phase crystallization [4] the process involves several additional phenomena such as the creation of crystalline seeds themselves, the influence of the oxide interface, the influence of strain, the influence of extended defects at the grain surface, etc. Also, a prevented nucleation of Si near the SiO_2 interfaces concerning the first adjacent 0.5–1.0 nm of the Si layer was reported [5]. An increase of the crystallization temperature was reported for different superlattices such as Si/SiO_2 superlattices [6–8], Ge/SiO_2 [9], and $Ge{:}H/GeN_x$ [10]. In this work we will show the general character of the increase in crystallization temperature for reduced layer thickness and discuss the origin of this retarded crystallization. In addition, we will demonstrate the impact of the arrangement of Si nanocrystals on the optical properties of Er doped structures.

2. Experiment

Amorphous Si/SiO_2 multilayers on crystalline Si substrates were prepared by RF sputtering and plasma oxidation with Si thickness varied from 1.9 to 20 nm and a constant thickness of the amorphous SiO_2 ($\sim$ 3 nm). Furnace annealing was used for crystallization in the temperature range of 700 to 1050°C. The temperature was raised by 50°C for each sample. The crystallization state was investigated by wide angle X-ray scattering, transmission electron microscopy (TEM), and high resolution TEM (for more details see Refs. [11,12]). In addition, Er and Si doping of high quality dry oxide were performed with doses of 1×10^{17} and 5×10^{14} cm^{-2}, respectively. Crystallization and Er^{3+} activation were done by thermal annealing at 1100°C (1 h) under N_2 atmosphere. Rutherford backscattering (RBS) measurements were performed using 2 MeV He^+ ions at a backscattering angle at 170°. Photoluminescence (PL) measurements were done at room temperature with a charged coupled diode (CCD) matrix array and a Ge detectors for detection and an Ar ion laser for excitation. The spectra are corrected with respect to the spectral response of the measurement system.

3. Results and discussion

3.1. Exponential increase of the crystallization temperature

Fig. 1 summarizes the crystallization temperature of an ensemble of superlattices based on different materials and interfaces as a function of layer thickness. An exponential increase in crystallization temperature was found while decreasing the layer thickness in all these different systems which was fitted by

$$T_c = T_{ac} + (T_{melt} - T_{ac})e^{-d/C}. \quad (1)$$

T_{melt} represents the melting temperature of bulk crystalline material, T_{ac} is the crystallization temperature of a thick bulk amorphous film, and d is the real thickness of the layer [12]. The lines in Fig. 1 represent a data fit using the above equation and parameters summarized in Table 1.

In addition, we found that the inhomogeneous strain of the Si/SiO_2 films at the crystallization temperature T_c depends exponentially on the Si layer thickness [6]. Hence, strain as well as crystallization temperature show a similar dependence on the Si layer thickness. In case of thick amorphous films the kinetics of the amorphous to polycrystalline phase transition was described previously by classical nucleation theory [4]. However, an amorphous SiO_2 interface on both sides of a thin Si layer (below 50 nm) will not result in a homogeneous and uninfluenced nucleation within the layers. Similar as in Refs. [8,9], we assume here that the crystallization nucleus is cylindrical in shape and symmetrically embedded in the amorphous material

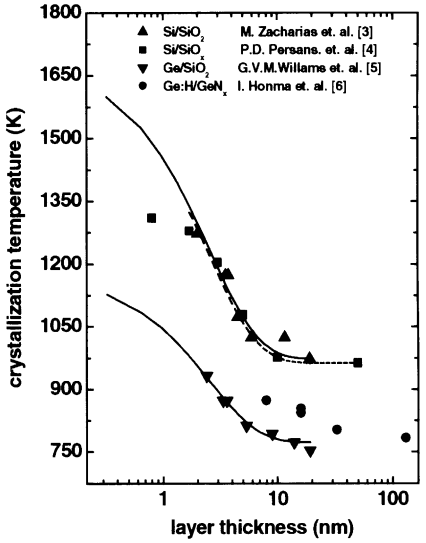

Fig. 1. Dependence of the crystallization temperature on the layer thickness.

Table 1
Used fitting parameter for lines in Fig. 1

Superlattice material	T_{melt} (K)	T_{ac} (K)	C (nm)
Si/SiO_2 (curve 1)	1683	973	2.56
Ge/SiO_2 (curve 2)	1211	773	2.52

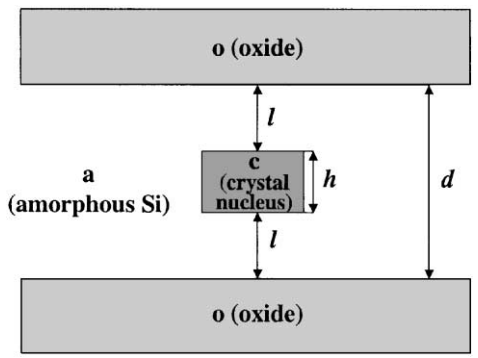

Fig. 2. Finite separation of a nucleus from oxide boundary.

between the oxide interfaces. However, we introduce an additional space l which corresponds to a finite separation of the nucleus from the oxide boundaries as can be seen in Fig. 2.

In principle, for each combination of phases we assume that a well defined, i.e. a sharp and perfect interface bounded by bulk material can be formed, which is characterized by its specific free interface energy. We define γ_{ac}, γ_{oc}, and γ_{oa} as the specific interfacial free energies per unit area between the different material phases. However, for the sandwich structure considered here, the interfaces between material o and material c are not well defined if the distance l between these materials is in the order of only a few lattice constants. For $l=0$, that is $h=d$, the Persans model should be re-derived. In the other limit, for l very large ($l \to \infty$), the materials o and c are separated by two non-interacting, well defined interfaces. In order to rationalize the interaction between these two interfaces for small l, an effective interface energy is defined, which interpolates between the above well defined limiting cases. For more details please see Ref. [6]. Hence, we write

$$\gamma_{oc}^{eff} = \gamma_{ac} + (\gamma_{oc} - \gamma_{ac})M \quad \text{with } M = e^{-l/l_0} \tag{2}$$

as an effective order parameter which is normalized to unity for the true oxide/crystalline interface and zero for the true amorphous/crystalline interface. In view of the exponential dependence of the inhomogeneous strain on layer thickness, M is expected to be an exponentially decreasing function of the interface spacing l. Assuming short range interatomic forces, l_0 can be interpreted as an average screening or bonding length which is related to the range of interatomic forces typical for the materials o and c. The nucleation energy barrier is then given by the difference of the Gibbs free energies:

$$\begin{aligned}\Delta G &= G_c - G_a \\ &= -\pi r^2 h\,\Delta G_v + 2\pi r h \gamma_{ac} + 2\pi r^2\,\Delta\gamma_{eff},\end{aligned} \tag{3}$$

with

$$\Delta G_v = G_{va} - G_{vc} > 0 \quad \text{and}$$

$$\Delta\gamma_{eff} = \gamma_{ac} + (\gamma_{oc} - \gamma_{ac} - \gamma_{oa})e^{-l/l_0}.$$

The terms in Eq. (3) describe the change in bulk free energy, the energy necessary for forming the new a/c interface, and the influence of the boundaries formed by the oxide material o, respectively. l is given by $l=(d-h)/2$, with $d \geqslant h$. Eq. (3) represents a generalization of the nucleation model of Persans et al. [8] which can easily be re-derived if $l=0$ (or $h=d$) is chosen in Eq. (3). For $\gamma_{oc} - \gamma_{oa} > 0$ the crystal nucleation is inhibited, but $\gamma_{oc} - \gamma_{oa} < 0$ will enhance

the formation of crystal nuclei. However, fixing the height h of the nucleus with the interface from the very beginning as used in Refs. [8,9] leads to a wrong behavior of the maximum value of ΔG as a function of d. In our model h and d are *geometrically independent parameters* which are coupled *energetically* by the above equation. This allows us to consider the Gibbs free energy change in Eq. (3) as a function of both the variables r and h. Due to the fact that the specific interface energies are not well known we make the following approximation: We ignore the fact that $\Delta\gamma_{\mathrm{eff}}$ depends on the size h of the nucleus and replace l by an average value $\bar{l} = (l_{\min} + l_{\max})/2 = d/4$. With this approximation and under the assumption that the right circular cylinder of radius r and height h in Fig. 2 corresponds to the equilibrium shape of the critical nucleus the radius-to-height ratio $r/h = \gamma_{\mathrm{ac}}/2\Delta\gamma_{\mathrm{eff}}$ can be derived by minimizing the Gibbs free interface energy in Eq. (3) under the constraint of a constant volume. Using this relation to eliminate one of the two variables in Eq. (3), i.e. r, the nucleation barrier is given by the maximum of ΔG: $\partial\,\Delta G/\partial h = 0$, yielding $r^* = 2\gamma_{\mathrm{ac}}/\Delta G_{\mathrm{v}}$ and $h^* = 4\Delta\gamma_{\mathrm{eff}}/\Delta G_{\mathrm{v}}$ for the critical radius and the critical cylinder height of the nucleus. Inserting r^* into Eq. (3) yields for the nucleation barrier $\Delta G^* = 8\pi\gamma_{\mathrm{ac}}^2\,\Delta\gamma_{\mathrm{eff}}/\Delta G_{\mathrm{v}}^2$ with $\Delta\gamma_{\mathrm{eff}}$ given by $\Delta\gamma_{\mathrm{eff}} = \gamma_{\mathrm{ac}} + (\gamma_{\mathrm{oc}} - \gamma_{\mathrm{ac}} - \gamma_{\mathrm{oa}})\mathrm{e}^{-d/4l_0}$. The nucleation rate is essentially proportional to the Boltzmann factor, $N \sim N/t \sim \exp(-\Delta G^*/kT)$, which means that the time t for the formation of a certain number N of nuclei is given by $t/N \sim \exp(\Delta G^*/kT)$. If we define the crystallization temperature T_{c}, as usual, by the requirement that a certain fixed number N_{c} of nuclei is generated at a given fixed time t_{c}, the crystallization temperature follows as

$$\frac{\Delta G^*}{kT_{\mathrm{c}}} = \ln\left(\frac{t_{\mathrm{c}}}{N_{\mathrm{c}}}\right) + \text{const.} \quad \text{or} \quad kT_{\mathrm{c}} \sim \Delta G^*.$$

Assuming now the bulk crystallization temperature T_{ac} by $kT_{\mathrm{ac}} \sim \Delta G_{\mathrm{ac}}^*$, with $\Delta G_{\mathrm{ac}}^* = 8\pi\gamma_{\mathrm{ac}}^3/\Delta G_{\mathrm{v}}^2$ as the bulk nucleation barrier derived for $d \to \infty$ we obtain

$$\frac{T_{\mathrm{c}}}{T_{\mathrm{ac}}} = \frac{\Delta G^*}{\Delta G_{\mathrm{ac}}^*} \quad \text{or}$$

$$T_{\mathrm{c}} = T_{\mathrm{ac}}\frac{\Delta\gamma_{\mathrm{eff}}}{\gamma_{\mathrm{ac}}} = T_{\mathrm{ac}}\left(1 + \frac{\gamma_{\mathrm{oc}} - \gamma_{\mathrm{ac}} - \gamma_{\mathrm{oa}}}{\gamma_{\mathrm{ac}}}\mathrm{e}^{-d/4l_0}\right). \tag{4}$$

This result already has the functional form of empirical Eq. (1). Comparison with Eq. (1) yields $T_{\mathrm{melt}} = T_{\mathrm{ac}}(\gamma_{\mathrm{oc}} - \gamma_{\mathrm{oa}})/\gamma_{\mathrm{ac}}$ and $C = 4l_0$. The crystallization temperature T_{c} experimentally observed tends to the temperature of the melting point of bulk crystalline silicon $T_{\mathrm{melt}} = 1683$ K in the limit of zero Si layer thickness, whereas in the thick layer limit we get $T_{\mathrm{c}}(d \to \infty) \approx T_{\mathrm{ac}} = 973$ K as was mentioned before [6]. Similar results were obtained for germanium (see Table 1). According to our theoretical results, the enhancement of T_{c} in the limit $d \to 0$ is related to the difference in the specific interface energies of the interfaces between the involved crystalline and amorphous phases. However, taking into consideration that the melting of the crystalline phase is likewise associated with the nucleation of a crystalline-to-liquid interface, the above results at last give us a hint why the crystallization temperature T_{c} for $d \to 0$ and the melting point T_{m} of the crystalline phase are in such a good empirical correlation. The screening length l_0 should be related to the range of interatomic forces or to the length of elastic interactions between the respective interfaces. We found $C \approx 2.52$–2.56 nm independent of the material (Ge,Si). Hence, the screening length is given by $l_0 \approx 0.64$ nm, which would correspond to a range of 2–3 interatomic distances using the lattice parameter of Si and Ge.

The minimum lateral radius r^* of the cylindrical nucleus, which is only determined by γ_{ac} and the change in the bulk Gibbs free energy per unit volume ΔG_{v}, is in the present approximation the same as the radius of a free spherical crystalline nucleus in bulk amorphous silicon. With $\Delta G_{\mathrm{v}} = \Delta g_{\mathrm{v}}/a^3$, where $\Delta g_{\mathrm{v}} = 0.100$ eV/atom is the free energy change associated with the crystallization of one atom [4], and $\gamma_{\mathrm{ac}} = \sigma_{\mathrm{ac}}/a^2$ with the amorphous/crystalline interface energy per atom $\sigma_{\mathrm{ac}} = 0.105$ eV/atom [4] we derive from the above equations $r^* = (2\sigma_{\mathrm{ca}}/\Delta g_{\mathrm{v}})a = 0.567$ nm (4–5 atoms per diameter). That means, the base area of the critical cylinder consists of only 17 atoms if we use an average interatomic distance of $a = 0.27$ nm for the Si atoms. The minimum height h^* of the cylindrical nucleus depends, via the effective specific interface energy, exponentially on the layer thickness. For thick layers bulk behavior is restored yielding $h^* = h_{\mathrm{bulk}}^* = 4\gamma_{\mathrm{ac}}/\Delta G_{\mathrm{v}} = 2r^* = 1.134$ nm for $d \to \infty$, which corresponds to a fairly symmetrical

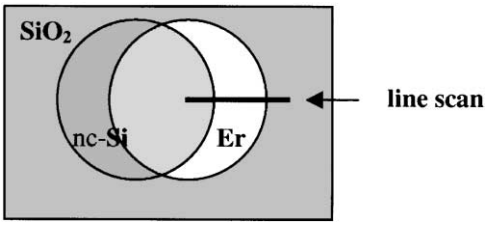

Fig. 3. Er and Si doping into thermal SO_2.

nucleus with the same volume as a spherical nucleus with radius r^*. For very small layer thicknesses the condition $l \geqslant 0$, i.e., $h^* \leqslant d$ must be fulfilled in our model (see Fig. 2), which gives a lower bound $d_{\min}$. In order to determine $d_{\min}$ we rewrite h^* in the form

$$h^* = 2r^* \left(1 + \left(\frac{\gamma_{oc} - \gamma_{oa}}{\gamma_{ac}} - 1\right) e^{-d/4l_0}\right).$$

Further, using the numerical values available [8], we expect no crystallization for layer thickness $d < d_{\min} \approx 1.6$ nm for the a-Si/SiO_2 system whatever the temperature. This is in good agreement with our measurements on the Si/SiO_2 system, where crystallization has been observed down to $d \approx 1.9$ nm. The value of $d_{\min} = 1.6$ nm is also larger than one would expect from purely geometrical considerations, which yields $d_{\min} = 1.1$ nm. The higher value of $d_{\min} \approx 1.6$ nm is clearly a consequence of a strong increase in the nucleation barrier caused by the continuous increase of the effective specific interface energy when the a/c and the o/c interfaces approach each other.

3.2. Er doping of Si nanostructures

Er and Si doping were performed into high quality oxide as shown in Fig. 3. Spatial separated areas containing Er ions, or Er ions in the vicinity of nc-Si are prepared on the same sample allowing a direct comparison of the properties using scanning techniques. Our measurements (PL,RBS) are along the black line of the figure and represent a line scan over the region of interest. The results of our PL measurement are directly compared with the doping profile by RBS spectra in Fig. 4. As clearly can be seen in Fig. 5, by mapping the color coded PL intensity along the line scan, we have a weak room temperature luminescence at 1.54 μm in pure oxide which is enhanced by nearly two orders of magnitude after crossing over

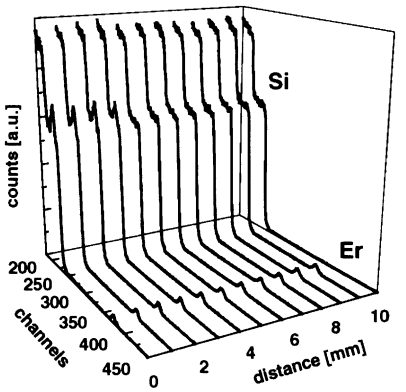

Fig. 4. Spatial resolved RBS spectra along the line scan.

to the region co-implanted with Si. At the same time the red Si luminescence decreases in intensity. This demonstrates without doubt the participation of the Si nanocrystals in the excitation route of the Er^{3+} states. In addition, Fig. 4 demonstrates the homogeneous doping profile of Er and Si ions by selected RBS spectra. Hence, the changes in PL intensity, shown in more detail in the selected spectra of Fig 6, are not caused by fluctuations in dopant profile but due to the interaction and the competition between different radiative processes. The results also prove that the excitation of the Er^{3+} state is mediated by the excitation of the nanocrystals. The shape of the observed Er luminescence shows a Stark splitting, which reflects the crystal field and hence the chemical surrounding of the active Er sites. This splitting suggests that the emitting Er ions are in the SiO_2 and not within nanocrystalline Si.

If an exciton recombines in a nanocrystal, the energy is emitted as a photon. However, a sufficient number of excitons transfer their energy to the Er ions either due to an Auger process, due to a dipole–dipole coupling or mediated by an intrinsic luminescence center located at the surface of the nanocrystals. That would explain the complementary behavior of the PL intensities of nc-Si and Er. In fact, the three different processes are in competition and for 1.54 μm based devices a way must be found to make the excitation of the Er^{3+} state the favorite route for energy transfer.

To exclude the intrinsic luminescence center at the surface of the nanocrystals we suggest a hydrogen treatment of the samples, which has not been done so far. In this way hydrogen might saturate surface

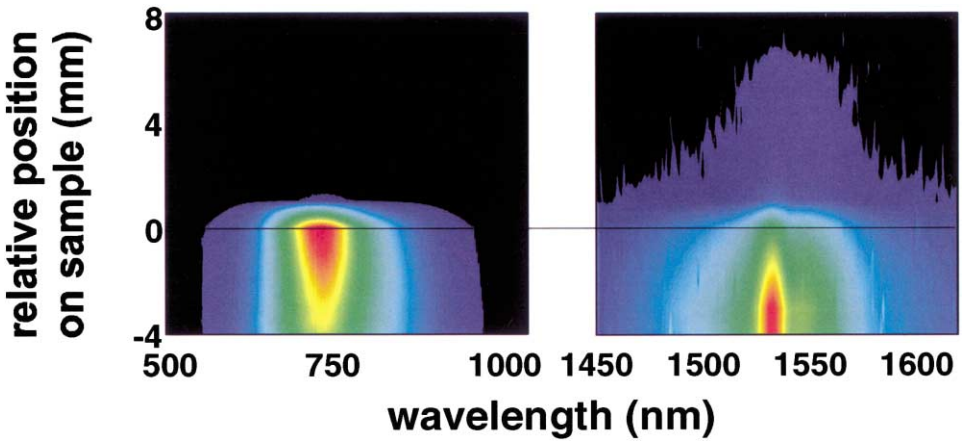

Fig. 5. Color coded PL intensity as a function of position on the sample monitoring first the pure oxide, than the oxide contaning Er and finally starting at the black line probing the region containg Er and nanocrystals. The left figure is due to the red luminescence of Si nanocrystals, the right figure presents the 1.54 μm luminescence of Er^{3+}.

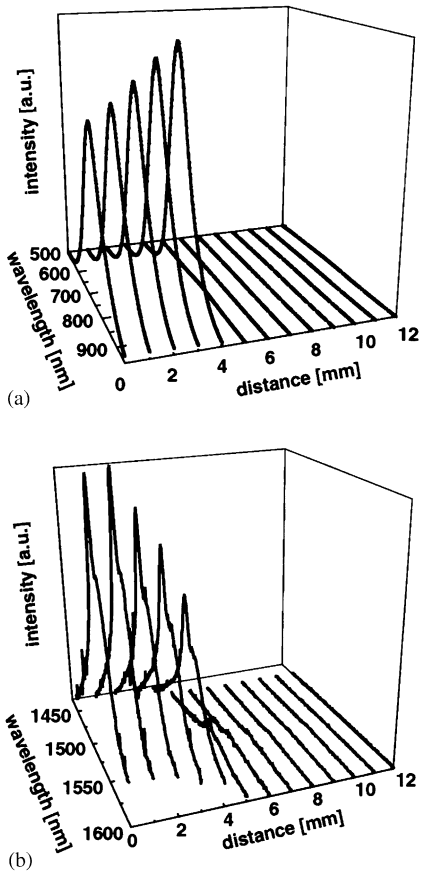

Fig. 6. (a) Spatial resolved PL of the Si nanocrystals along the line scan. (b) Spatial resolved Er^{3+} luminescence measured along the line scan.

defects closing this path. The temperature dependence of the rare earth luminescence was investigated and found to be very weak with a quenching of a factor of two for temperature down to 4 K [13]. This can be explained by means of low level non-radiative de-excitation for the material and is in agreement with values reported by other authors [14].

4. Conclusions

The novel concept of an effective interface energy is applied to the Si/SiO_2 system that interpolates between the true oxide/crystalline interface energy and the true amorphous/crystalline interface energy by means of an order parameter varying continuously with interface spacing. The exponential increase of the crystallization temperature with decreasing layer thickness is derived using crystallization theory and taking into account the different interface energies and materials. The model yielded a lower bound for the layer thickness below which no crystallization can occur for the Si/SiO_2 system. The exponential scaling of crystallization temperature and layer thickness for $(Si, Ge)/SiO_2$ superlattices is shown from experiments and theory. This behavior is reduced to basic material properties like the bulk amorphous crystallization temperature and the melting point.

In addition, we have reported spatial resolved investigations of Er doped SiO_2 films co-implanted with

Si and combined with spatial resolved RBS investigations along the same line scan. Our results clearly prove that the dramatic change in PL intensity by two orders of magnitude cannot be explained by inhomogeneities of the implantation. We suggest that the Er ions are excited very efficiently through energy transfer involving excitons confined within the nanocrystals.

Acknowledgements

The authors are grateful for financial support from the Volkswagen Stiftung and the DFG and wish to thank Prof. J. Christen (University of Magdeburg) and Prof. T. Butz (University of Leipzig) for the possibility to use the equipment of their institutes.

References

[1] L. Pavesi, L. Dal Negro, C. Mazzoleni, G. Franzò, F. Priolo, Nature 408 (2000) 440.
[2] Z.H. Lu, D.J. Lockwood, J.-M. Baribeau, Nature 378 (1995) 258.
[3] L. Tsybeskov, K.D. Hirschman, S.P. Duttagupta, M. Zacharias, P.M. Fauchet, J. McCaffrey, D.J. Lockwood, Appl. Phys. Lett. 72 (1998) 43.
[4] C. Spinella, S. Lombardo, F. Priolo, J. Appl. Phys. 84 (1998) 5383.
[5] J. Gonzalez-Hernandez, R. Tsu, Appl. Phys. Lett. 42 (1983) 90.
[6] M. Zacharias, P. Streitenberger, Phys. Rev. B 62 (2000) 8391.
[7] Z.H. Lu, Solid State Electron. 40 (1996) 191.
[8] P.D. Persans, A. Ruppert, B. Abeles, J. Non-Cryst. Solids 102 (1988) 130.
[9] G.V.M. Willams, A. Bittar, H.J. Trodah, J. Appl. Phys. 67 (1990) 1874.
[10] I. Honma, H. Hotta, K. Kawai, H. Komiyama, K. Tanaka, J. Non-Cryst. Solids 97&98 (1987) 947.
[11] J. Bläsing, P. Kohlert, M. Zacharias, J. Appl. Crystallogr. 31 (1998) 589.
[12] M. Zacharias, J. Bläsing, K. Hirschman, L. Tsybeskov, P.M. Fauchet, J. Non-Cryst. Solids 266–269 (2000) 640.
[13] M. Schmidt, J. Heitmann, M. Zacharias, Thin Solid Films, in press.
[14] G. Franzò, V. Vinciguerra, F. Priolo, Appl. Phys. A 63 (1999) 3.